Applied Catalysis A, General 561 (2018) 150–157

Contents lists available at ScienceDirect

Applied Catalysis A, General

journal homepage: www.elsevier.com/locate/apcata

Stability of gold nanocatalysts supported on mesoporous silica for the oxidation of 5-hydroxymethyl furfural to furan-2,5-dicarboxylic acid

Nazila Masoud[1], Baira Donoeva[1], Petra E. de Jongh*

Inorganic Chemistry and Catalysis, Debye Institute for Nanomaterials Science, Utrecht University, Universiteitsweg 99, 3584 CG Utrecht, The Netherlands

ARTICLE INFO

Keywords:
Gold catalysis
Support morphology
Particle growth
Nanoparticles
Selective oxidation

ABSTRACT

The synthesis of furan-2,5-dicarboxylic acid via catalytic oxidation of 5-hydroxymethyl furfural is an important step for the production of bio-sourced polymers. We report on the activity of SiO_2-supported Au catalysts for this reaction. These catalysts reached 74% furan-2,5-dicarboxylic acid yield at 90 °C in 5 h when 5-hydroxymethyl furfural to Au molar ratio was 72. We also investigated the influence of the morphologies of the silica supports on the growth of Au nanoparticles under reaction conditions. Pronounced growth of Au nanoparticles occurred on Aerosil, SiO_2 with a disordered porosity and 50 nm average pore diameter: Au nanoparticles grew from 2.4 to 10.1 nm. However, by using ordered mesoporous supports, the growth of the gold nanoparticles was successfully minimized. Also the reaction conditions influenced the particle growth; for instance using HCO_3^- as a base led to more pronounced particle growth than using NaOH. Particle diffusion in solution, and subsequent coalescence and agglomeration was proposed to be the dominant particle growth mechanism. Our results show the importance of support morphology in mitigation of Au particle growth in liquid phase oxidation reactions.

1. Introduction

Furan-2,5-dicarboxylic acid (FDCA) can be used as a renewable building block for the production of polymers like polyesters, polyamides, and polyurethanes [1–3]. For example, FDCA reacts with ethylene glycol to form polyethylene furanoate which is a bio-based polymer. Production of FDCA via catalytic oxidation of 5-hydroxymethyl furfural (HMF) has been widely studied, using air or O_2 as the oxidant and typically under basic conditions. Commercialization of the FDCA production is planned by BASF and Avantium, based on a process involving Co/Mn/Br homogeneous catalysts [4,5]. The design of a heterogeneous catalyst that fulfills the industrial requirements is however highly desirable.

The quest is for catalysts that allow the oxidation of HMF, which contains an alcohol and an aldehyde group, to FDCA, which contains two acid groups [6]. The reaction occurs in consecutive steps via a 5-hydroxymethyl furan carboxylic acid (HMFCA) intermediate, if Au is used as a catalyst (Scheme 1). Supported metal catalysts, for instance Pt [6–11], Pd [12–17], Ru [18,19], and Au [20–22] have been extensively studied for this reaction. Different reaction conditions and different catalysts lead to different activities. In general, higher metal to HMF ratios [23], more alkaline conditions [20,23], and smaller metal nanoparticles [24,25] lead to higher activities of the supported metal catalysts. It is also reported that the chemical nature of the support can affect the catalytic activity [10,20,22,26–29].

Gold catalysts are more active than Pt, Ru, and Pd [3,23,26], or according to other reports, at least equally active to the other metal catalysts for this reaction [19,30]. Gold catalysts are more resistant than for instance Pt catalysts to poisoning [3,7,10] and leaching [6]. However, Au catalysts are prone to particle growth especially under oxidative conditions [31–36]. Au nanoparticles supported on carbon with 5 nm open pores grew upon HMF oxidation in the presence of $NaHCO_3$ (initial pH of 8–8.5), and the extent of particle growth depended on the surface properties of the support [37]. Casanova et al. suggested particle growth as a deactivation mechanism for Au/TiO_2 and Au/CeO_2 for HMF oxidation in the presence of NaOH as a base at 45 °C, though a full characterization of the spent catalysts and particle size after catalysis was not given [20]. Gupta et al. reported that Au/hydrotalcite is stable during oxidation of HMF at pH of 10 where the high pH was caused by solid basicity of support [22]. Gupta et al. also reported growth of Au on MgO in a base free condition, suggesting that particle growth depends on the support. Furthermore, Prüße et al. showed a long term stability of the Au on TiO_2 and Al_2O_3 during selective oxidation of glucose at 40 °C and in the presence of KOH or NaOH as a base at pH of 9 [38,39]. It is not clear from the literature which factors affect the particle growth. Hence, a detailed investigation

* Corresponding author.
E-mail address: P.E.deJongh@uu.nl (P.E. de Jongh).
[1] Both authors contributed equally.

https://doi.org/10.1016/j.apcata.2018.05.027
Received 22 February 2018; Received in revised form 21 May 2018; Accepted 23 May 2018
Available online 24 May 2018

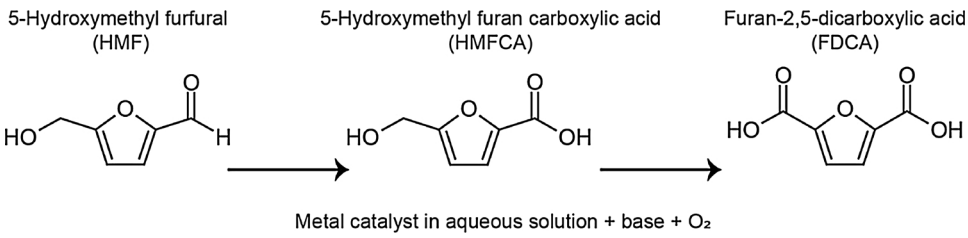

Scheme 1. Oxidation of 5-hydroxymethyl furfural (HMF) to furan-2,5-dicarboxylic acid (FDCA) via formation of intermediate 5-hydroxymethyl furan carboxylic acid (HMFCA).

of the factors that affect the stability of the Au nanoparticles as well as strategies to alleviate Au particle growth are needed.

Silica supports are widely used in heterogeneous catalysis [40,41]. They can be prepared with different specific surface areas (50–2000 m^2/g) and structures. For example, aggregated spherical particles of Aerosil form a porous material in which the pores are formed by interparticle spaces. Ordered mesoporous structures like SBA16 [42] and mesoporous cellular foam (MCF) [43] have cage like structures with different neck sizes. Like SBA16, silica gel can have small pore sizes (around 9 nm), but it has a disordered structure [44]. The flexibility in having supports with different surface areas and structures allows the design of catalysts with different interparticle distances and a uniform distribution of well-defined nanoparticles. Previously, our group reported for Cu nanoparticles on SiO_2 for methanol synthesis that a uniform distribution of nanoparticles which maximize interparticle distances minimizes particle growth [45,46]. It was also found that the neck size was a crucial factor to limit particle growth for these catalysts [44].

In this study, the activity and stability of Au on SiO_2 for liquid phase oxidation of HMF to FDCA are investigated. This is the first time that the activity of Au/SiO_2 for this reaction is reported. In general, carbon supports are better candidates for this type of reactions due to their higher hydrothermal stability in particular under alkaline conditions. However, diverse structures of the SiO_2 supports allow a detailed investigation of the effect of support morphology on the stability of Au nanoparticles. Our results show that the morphology of the support plays an important role in the stability of the SiO_2-supported Au catalysts.

2. Material and methods

2.1. Catalyst preparation

Aerosil 300 (BET surface area of 270 $m^2\,g^{-1}$, mesopore volume of 0.78 mL g^{-1}) was purchased from Evonik. Silica gel 7085 (BET surface area of 500 $m^2\,g^{-1}$, mesopore volume of 0.90 mL g^{-1}) was received from Grace Davison. Mesoporous SiO_2 supports (SBA16 and MCF) were prepared in house. MCF [43] was prepared by dissolving Pluronic P123 (2.0 g, $EO_{20}PO_{70}EO_{20}$, M_{av} = 5800, Sigma Aldrich) in aqueous HCl solution (75 mL, 1.6 M) at room temperature (RT). Then, 1,3,5-trimethylbenzene (TMB, 2.0 g) was added. After stirring at least 45 min at 35 °C, tetraethoxysilane (4.4 g, TEOS) was added, and the mixture was transferred to a 200 mL Teflon-lined autoclave. After 20 h at 38 °C in static condition, the cloudy suspension was further kept at 100 °C for 24 h in static condition. The precipitate was filtered and washed at RT until no chloride ions were left (verified using an $AgNO_3$ solution to test the washing liquid) and subsequently dried at 120 °C in static air overnight. Finally, the precipitate was calcined at 500 °C in static air for 6 h to yield MCF (BET surface area of 610 $m^2\,g^{-1}$, total pore volume of 2.01 mL g^{-1}).

SBA16 [42] was prepared by dissolving Pluronic F127 (4.7 g, $EO_{106}PO_{70}EO_{106}$, M_{av} = 12600, Sigma Aldrich) in a mixture of aqueous HCl solution (75 mL, 1.6 M) and water (210 mL) at RT. Then, 1-butanol (13.2 g) was added, and the mixture was stirred at 35 °C for 1 hour. Then, tetraethoxysilane (20.8 g, TEOS) was added dropwise under fast stirring. The mixture was transferred to a Teflon-lined autoclave, and after 20 h at 35 °C under static conditions, the cloudy suspension was subsequently kept at 100 °C for 24 h. The precipitate was filtered and washed at RT until no chloride ions were left, as evidenced by silver nitrate test, and subsequently dried at 120 °C in static air overnight. Finally, the precipitate was calcined at 540 °C in static air for 6 h to yield SBA16 (BET surface area of 780 $m^2\,g^{-1}$, total pore volume of 1.04 mL g^{-1}).

All supports (3 *g* for each of them) were functionalized using aminopropyl triethoxysilane (APTES). First, they were dried at 140 °C under vacuum for 24 h. Then, dry toluene (50 mL) and APTES (1 g for Aerosil and 3 g for silica gel, MCF and SB16) were added. We added the amount of APTES needed for covering the support surface based on the BET surface area of the supports, and considering three OH groups per nm^2 of the SiO_2 support [47]. The mixture was refluxed for 24 h at 110 °C in a N_2 atmosphere. The functionalized supports were recovered by centrifugation, washed with ethanol (40 mL) at RT twice, and dried at 60 °C in static air overnight.

All catalysts were prepared following the method of Mou et al. for the deposition of Au on SiO_2 [48]. The functionalized supports (1 g) were dispersed in water (15 mL, doubled distilled). To deposit 1.5 wt% Au on Aerosil and 3 wt% Au on Aerosil, silica gel, MCF, and SBA16, appropriate amount of an aqueous Au solution (0.06 M $HAuCl_4.3H_2O$, Sigma Aldrich) were added. The mixture was stirred at RT for two hours, and the powder was recovered by centrifugation and washed with H_2O (40 mL) at RT twice. Then, the powder was re-dispersed in water (15 mL) and reduced by a rapid addition of an excess of a reducing agent (10 mL, 0.2 M $NaBH_4$) under vigorous stirring at RT. After 20 min, the product was collected by centrifugation, washed with water (40 mL) at RT five times and dried at 60 °C in static air overnight. To eliminate the organic groups, the catalysts were calcined at 500 °C in static air for 4 h. The catalysts are denoted as Au/Aerosil, Au/silica gel, Au/MCF, and Au/SBA16.

2.2. Characterization

Elemental analysis was performed using inductively coupled plasma-optical emission spectrometry in the Faculty of Geosciences at Utrecht University. X-Ray Diffraction (XRD) was carried out with a Bruker D2 phaser with Co K_α source. Crystallite sizes were obtained from the peak broadening at $2\theta = 44°$ using the Scherrer equation. For transmission electron microscopy (TEM) imaging on MCF and SBA16 samples, they were first embedded in epoxy resin (Epofix, EMS), then cut to slides of 70 nm thickness using a Diatome 35° diamond knife mounted on an Ultracut E Reichert-Jung microtome (Leica) and finally collected on TEM grids. TEM imaging was performed on a Tecnai 12 (FEI) microscope operated at 120 kV. High angle annular dark-field scanning transmission electron microscopy (HAADF-STEM) was performed on a Talos F200X microscope operated at 200 kV. Energy-dispersive X-ray (EDX) spectroscopy was performed by four windowless SuperX EDX-detectors with a resolution of 128 eV arranged around the sample. STEM image processing and identification of the EDX signal was carried out using Tecnai Imaging Analysis (TIA) software. Particle sizes were determined from the TEM images by measuring the sizes of typically 300 particles on different places of the sample.

Nitrogen physisorption measurements were performed at −196 °C (Micromeritics, TriStar 3000) to determine the BET surface area of the

supports as well as the size distribution of the cage sizes and neck sizes for the MCF and SBA16 samples. The size distribution of the cage sizes was derived from the adsorption branch using the Barrett − Joyner − Halenda model modified according to the Faas correction for MCF and modified according to the Kruk − Jaroniec − Sayari correction for SBA16 [42]. The size distribution of the neck sizes was derived from desorption branch using the same model. An empirical form of the Harkins − Jura-de Boer equation was considered as a thickness reference curve [42].

To estimate the interparticle distances for Au on different SiO_2 supports and with different loadings, we first estimated the number of Au nanoparticles per surface unit by dividing the total number of Au atoms in the sample by the number of Au atoms in one particle [49] and by the BET surface area of the support. These calculations were based on determined XRD crystallite size. If evenly distributed, one can estimate that x nanoparticles per 10^6 nm^2 of support form arrays of $x^{0.5}$ nanoparticles on a square of $1000 \times 1000\,nm^2$ surface; therefore, average interparticle distances given in nm can be estimated by 1000 divided by $x^{0.5}$.

2.3. Catalytic tests

HMF (0.2 mmol), $NaHCO_3$ (0.4 mmol), and the catalyst (25 mg) were added to a 12 mL stainless steel autoclave containing 8 mL of deionized water. The autoclave was heated to 80 °C and pressurized with O_2 (10 bar) under vigorous stirring (900 rpm). During the reaction, 0.1 mL sample was taken at regular intervals of about 0.5–1 hours, filtered with 0.2 µm PTFE filters, diluted with water and analyzed using a high-performance liquid chromatograph (Shimadzu LC-20AD equipped a Bio-Rad Aminex HPX-87H column). Sulfuric acid (5 mM) at 333 K with a flow rate of 0.55 mL min^{-1} was used as an eluent. Each catalyst was tested at least twice to verify the reproducibility. The reproducibility of conversion levels and yields were within 5%.

3. Results and discussion

3.1. Structural characterization

Table 1 presents the structural properties of the Au catalysts on different SiO_2 supports. The BET surface areas of the Au/SiO_2 samples, pore sizes for the Aerosil and silica gel, and cage and the neck sizes for the MCF and SBA16 samples were obtained from the N_2 physisorption isotherms (Fig. 1). Silica gel, SBA16 and MCF had similar surface area which was two times larger than the surface area of Aerosil. Aerosil and silica gel had open pore structures with different pore diameters, 50 and 9 nm, respectively, but SBA16 and MCF had cage like pore structures in different sizes. SBA-16 has an ordered mesoporosity [42]. The different pore structures of the supports are visible in the transmission electron microscopy images (Fig. 2). The Aerosil had an open 3D pore structure, while the silica gel and SBA16 had much smaller pores and the MCF clearly showed the presence of pore cages.

Table 1
Characteristics of the as prepared Au supported on different mesoporous SiO_2.

Sample name	Au loading (wt%)	BET Surface area (m^2/g)	Cage size [a] (nm)	Neck size [a] (nm)	TEM particle size (nm)	XRD crystallite size (nm)
Au/Aerosil	2.2	230	50 [b]	–	2.3 ± 0.5	2.4
Au/Aerosil	1.3	230	50 [b]	–	2.2 ± 0.5	2.6
Au/silica gel	2.0	500	9 [b]	–	2.7 ± 1.1	2.8
Au/SBA16	2.6	420	9	7	3.3 ± 0.6	3.0
Au/MCF	2.4	430	26	15	3.0 ± 0.5	2.8

[a] Diameter.
[b] Average pore diameter.

Fig. 2 also show that nanoparticles with an average size range of 2.0–3.5 nm were deposited inside the pores of the mesoporous SiO_2 supports. Surface functionalization of the silica support with aminopropyl groups facilitated the preparation of small Au nanoparticles and a homogenous distribution over the support. Without the surface functionalization, large Au particles are formed. In X-ray diffraction patterns (Fig. 3a) peaks at $2\theta = 25°$ correspond to SiO_2 and peaks at 2θ of 44°, 52°, and 78° correspond to Au (111), (200), and (220), respectively. The crystallite sizes, as obtained from the peak broadening of the diffraction line at $2\theta = 44°$ varied from 2.4 to 3.0 nm confirming the particle sizes seen in TEM. In all cases, particle sizes are similar and the particles are much smaller than the pore sizes.

3.2. Catalytic performance

Fig. 4 shows the evolution of the HMF conversion and the FDCA yield. It shows that Au on all different SiO_2 supports was active for the conversion of HMF to FDCA. Full conversion of HMF, which contains an alcohol and an aldehyde group, was achieved in 2 h of reaction for all catalysts. Products were 5-hydroxymethyl furan carboxylic acid (HMFCA), which contains an alcohol and an acid group, the desired FDCA, which contains two acid groups, and a minor side product of 2,5-formylfurancarboxylic acid (FFCA), which contains an aldehyde and an acid group and it is an intermediate in the formation of FDCA from HMFCA. Notably, no activity was observed in the absence of $NaHCO_3$. If $NaHCO_3$ was added, the initial pH of the reaction mixture was 8.5. Upon reaction and production of the acid products, the pH slowly decreased to 7 after 6 h of catalysis, and, the product mixture consisted of 42–55 % FDCA. Reaction profiles were similar for the Au on different SiO_2 supports except that Au/silica gel is less active in FDCA formation probably due to different surface properties for the silica gel, for instance a different surface acidity. At a higher reaction temperature (90 °C), the FDCA yield was higher (74% for 2.2 wt% Au/Aerosil, Table 2, the first entry) as expected for an activated process, and in agreement with Casanova et al. [20]. who showed that higher temperatures up to 130 °C yields more FDCA.

The FDCA production was rather slow for our Au on SiO_2 catalysts compared to Au on reducible oxide supports reported in literature. Gorbanev et al. [50]. reported the NaOH-promoted aqueous oxidation of HMF using a Au/TiO_2 catalyst. Full conversion of HMF and a FDCA yield of 71% (HMF/Au mole ratio: 100, 20 equivalent of NaOH, 20 bar O_2, at 30 °C, in 18 h) were reached. Casanova et al. [20] demonstrated full conversion of HMF and a FDCA yield of > 99% for Au/TiO_2 and Au/CeO_2 catalysts (HMF/Au mole ratio: 150, 4 equivalent of NaOH, 10 bar O_2, at 65 °C, in 5 h). However in both examples, stronger base (NaOH) and higher base/HMF ratio were used, explaining the higher FDCA yield.

Gupta et al. reported that Au/SiO_2 in the absence of a base was inactive for the oxidation of HMF [22]. This is the first time that an activity of Au/SiO_2 for this reaction is reported. Table 2 gives a comparison of the catalytic properties of the current Au/Aerosil to literature results for Au on high surface area graphitic carbon supports with different surface functions, all tested under the same reaction conditions at 90 °C [37]. SiO_2 has point of zero charge (PZC) of 2–4 [51], close to that of carbon support with PZC of 4.0, though surface group density is higher on SiO_2 than the carbon. Au/SiO_2 is much more active in FDCA production than Au on that carbon support. The activities of Au/SiO_2 and Au/C with a PZC of 9.9 are close. Generally, the activity of carbon-supported Au catalysts for FDCA production is strongly affected by the surface groups present on the carbon supports [37]. The comparison of SiO_2-supported Au catalysts to those on reducible oxide supports (which show higher activity) and to those on carbon supports (which show a lower activity under similar conditions) shows that our first results on SiO_2 are in line with the literature results on other supports, although it is clear that the chemical nature of the support plays an important role in determining the activity of the supported Au catalysts.

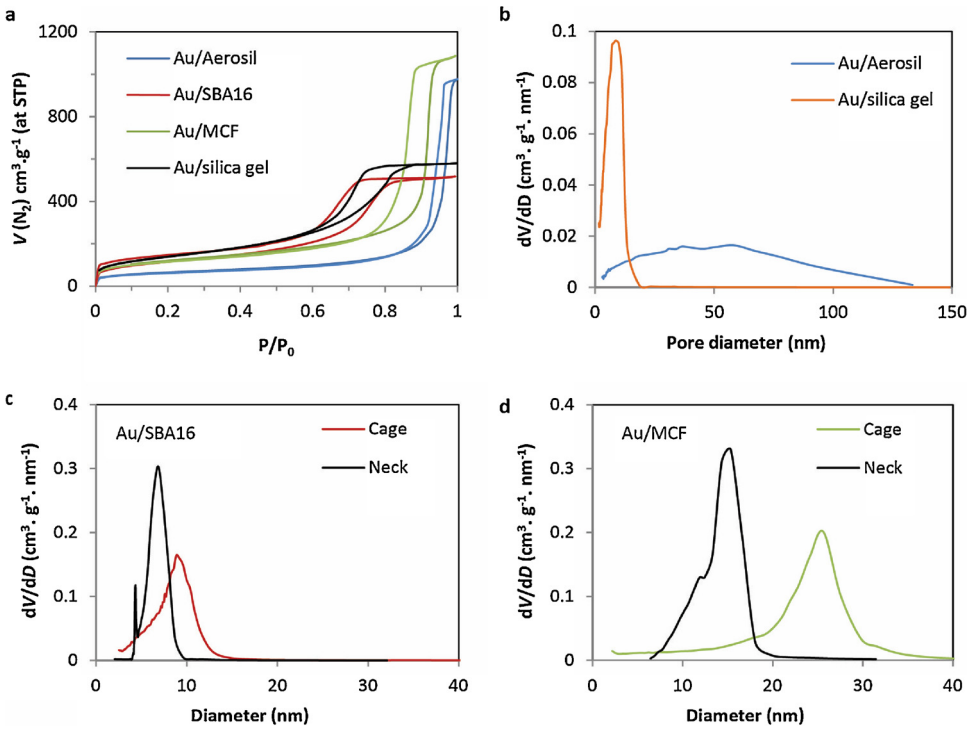

Fig. 1. Nitrogen adsorption-desorption isotherms for Au/Aerosil, Au/silica gel, Au/MCF, and Au/SBA16 samples (a), differential pore diameter distribution for Au/Aerosil and Au/silica gel (b), and distribution of cage and neck diameter sizes for Au/SBA16 (c) and Au/MCF (d).

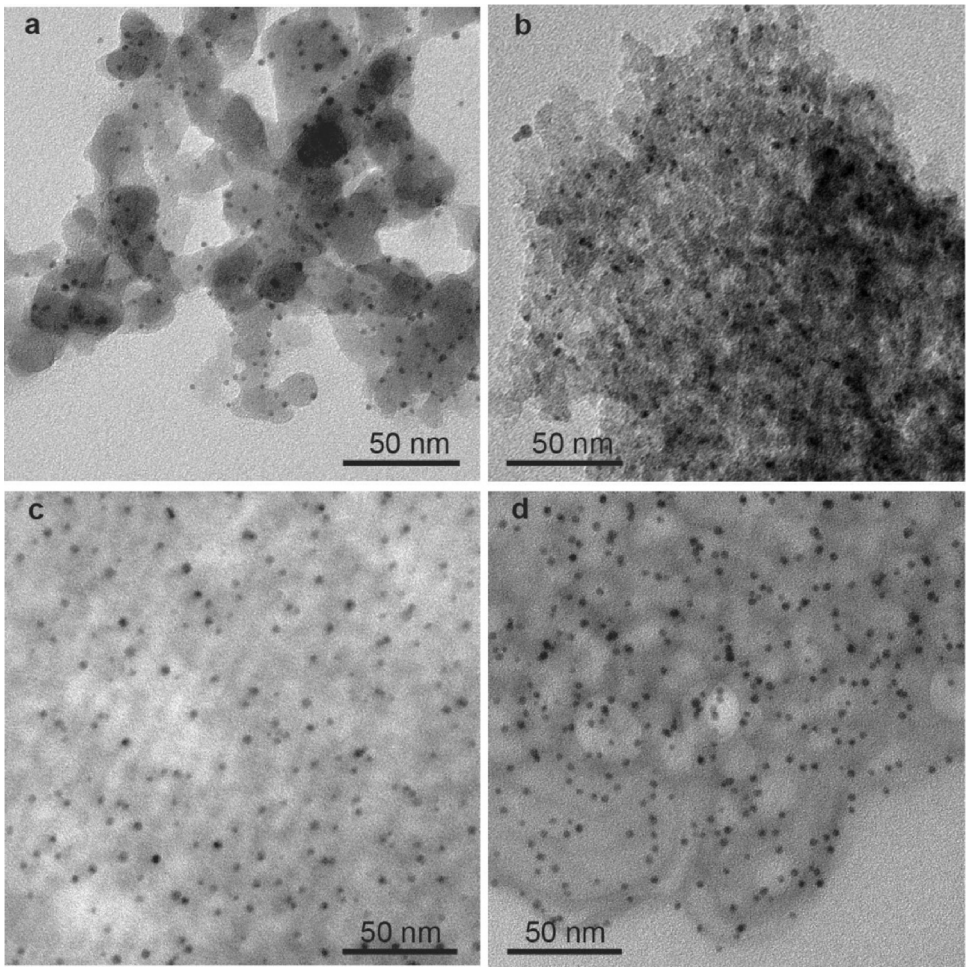

Fig. 2. TEM micrographs of a) 2.2 wt% Au/Aerosil, b) 2.0 wt% Au/silica gel, c) 2.6 wt% Au/SBA16, and d) 2.4 wt% Au/MCF.

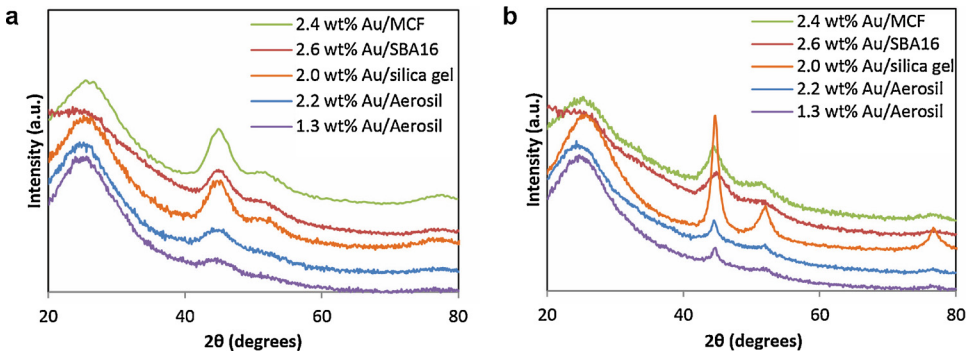

Fig. 3. X-ray diffraction patterns of Au on Aerosil, silica gel, MCF, and SBA16 a) before, and b) after 6 h of catalysis. Peaks at 2θ = 25° correspond to SiO_2 and peaks at 2θ of 44°, 52°, and 78° correspond to Au (111), (200), and (220), respectively.

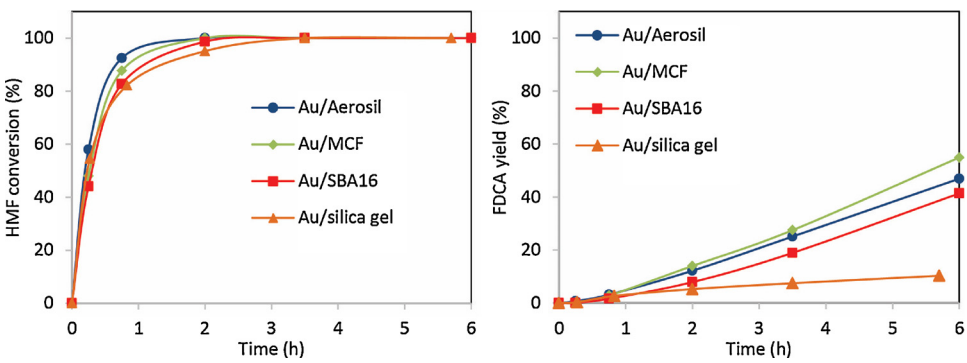

Fig. 4. Evolution of HMF conversion (left) and FDCA yield (right) catalyzed by the Au on different SiO_2 supports. Conditions: HMF (0.2 mmol), catalyst (2.2–2.6 wt% Au/SiO_2, 25 mg Au/Aerosil, 17 mg Au/MCF, 17 mg Au/SBA16, or 17 mg Au/silica gel, HMF to Au mole ratio is 72–97), $NaHCO_3$ (0.4 mmol), H_2O (8 mL), O_2 (10 bar), at 80 °C, 900 rpm stirring.

Table 2
HMF oxidation in the presence of Au catalysts on different supports. Conditions: HMF (0.2 mmol), catalyst (25 mg of 2.2 wt% Au/Aerosil, HMF to Au mole ratio is 72), $NaHCO_3$ (0.4 mmol), H_2O (8 mL), O_2 (10 bar), at **90** °C, 900 rpm stirring, HMF conversion was always > 99%.

Catalyst	TEM particle size (nm)	HMFCA yield (%)	FDCA yield (%)	Reference
Au/Aerosil	2.3 ± 0.5	21 [a]	74 [a]	This work
Au/C (PZC of 4.0)	3.3 ± 1.1	93 [b]	6 [b]	ref. [37]
Au/C (PZC of 9.9)	2.4 ± 0.7	22 [b]	75 [b]	ref. [37]

[a] Yield was calculated after 6 h of catalysis.
[b] Yield was calculated after 12 h of catalysis.

A direct comparison of FDCA productivities is not possible, because of different reaction conditions (pH, HMF/Au molar ratio, temperature, reaction time, and different bases). Nevertheless from our comparison it seems that Au/SiO_2 has a comparable or higher activity than previously reported Au catalysts supported on carbons and other metal oxides.

3.3. Stability

Fig. 3 shows the XRD patterns of Au on different SiO_2 supports before and after 6 h of catalysis, and Fig. 5 shows the TEM images of the catalysts after 6 h of catalysis. Table 3 summarizes the sizes of the Au nanoparticles before and after catalysis as characterized by TEM and XRD. The average crystallite size for the spent 2.2 wt% Au/Aerosil was 10 nm which proofs a pronounced particle growth, and the corresponding XRD peak showed two components which suggest a bimodal particle size distribution. Au/Aerosil catalyst with a lower Au loading (1.3 wt%) grew to a similar size (to 10.5 nm). TEM images of the spent Au/Aerosil catalysts showed large particles as well as the 2–3 nm Au particles.

Dark-field TEM images of the spent Au/Aerosil (Fig. 6a) showed the presence of a few large agglomerates of Au particles of 10–30 nm. Energy-dispersive X-ray spectroscopy confirmed that these agglomerates contain Au (Fig. 6b). The presence of both small and large particles did not allow an accurate determination of the average particle size from the TEM images.

The average crystallite size for the spent Au/silica gel was 8.5 nm (Fig. 3b and Table 3), hence these particles grew extensively although less than those on Aerosil. Corresponding TEM images confirmed the particle growth for the Au/silica gel (Fig. 5). For Au on SBA16 and MCF supports, comparison of the crystallite sizes and particle sizes, before and after catalysis (Table 3 and Fig. 5) showed that they were much more stable (growth to 4.5 nm). TEM images of Au on MCF and SBA16 after catalysis (Fig. 5) showed limited particle growth, and no large particles were observed on these spent catalysts. Data regarding the long-term stability of the Au/SBA16 are presented in the supporting information S.1. It shows that the SiO_2 support does not withstand long-term exposure to these basic reaction conditions. Moreover, upon degradation of the ordered SiO_2 structure, large Au nanoparticles were formed. Nevertheless, the turnover frequencies for HMF conversion and FDCA formation remained constant during catalysis in the three cycles. This suggests that the loss of activity is just because of the increase in particle size, and hence loss of active surface area, but that there is no change in the nature of the active sites. It further suggests that particle size has no significant effect on the catalytic activity in the particle size range tested.

The question is first why the growth of Au nanoparticles is influenced by the type of silica supports, and second, what the role of the support structure is on Au particle stability.

3.3.1. Reaction parameters affecting particle growth

To answer the first question, we first discuss the factors that affect the growth. To understand, in more detail, the growth of Au nanoparticles during the reaction, Au/Aerosil catalyst that encountered the most pronounced particle growth was analyzed under different reaction conditions. Particle growth was limited after 6 h exposure of the Au/Aerosil catalyst to the reaction mixture that contains HMF in an

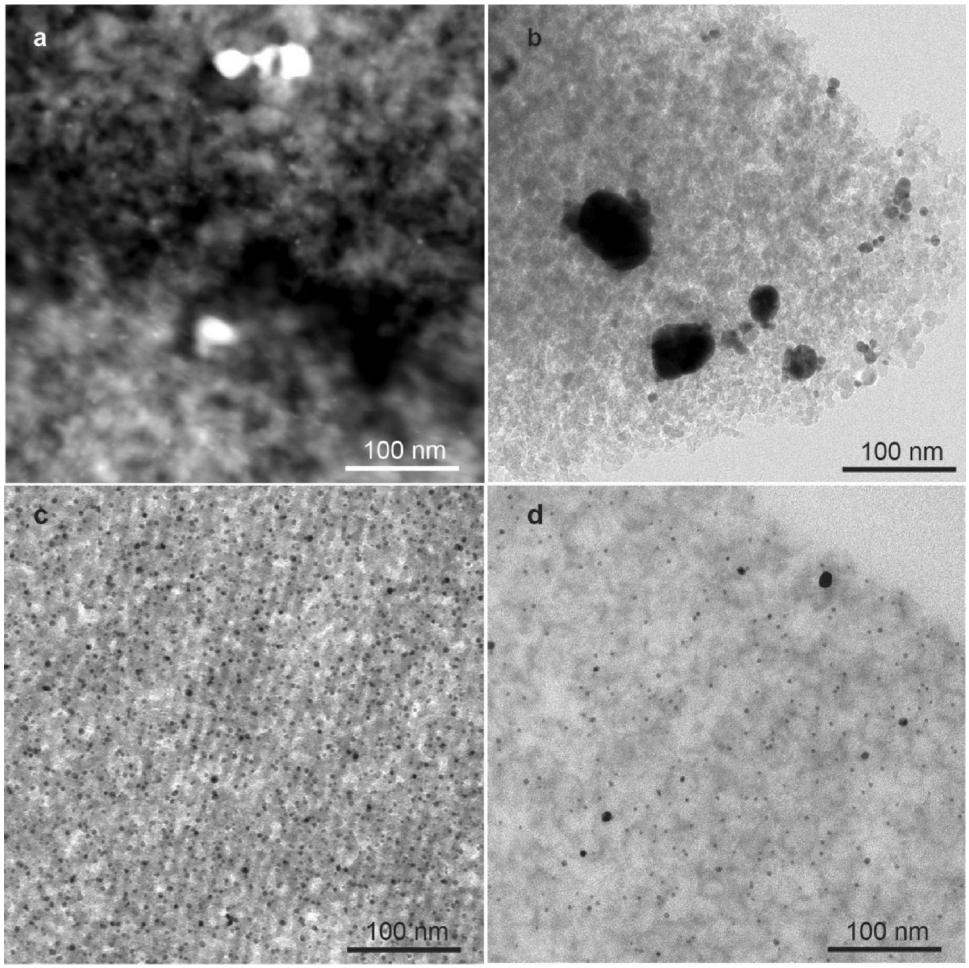

Fig. 5. a) High angle annular dark-field STEM images of 2.2 wt% Au/Aerosil, and bright field TEM images of b) 2.0 wt% Au/silica gel, c) 2.6 wt% Au/SBA16 and d) 2.4 wt% Au/MCF the after 6 h of catalysis.

Table 3
Changes in the size of Au nanoparticles on different SiO_2 supports and with different Au loadings upon 6 h of catalysis. Conditions: HMF (0.2 mmol), catalyst (1.3–2.6 wt% Au/SiO_2, 25 mg, HMF to Au mole ratio is 60–120), $NaHCO_3$ (0.4 mmol), H_2O (8 mL), O_2 (10 bar), at 80 °C, 900 rpm stirring.

Sample name	Crystallite size before catalysis (nm)	Particle size before catalysis (nm)	Crystallite size after catalysis (nm)	Particle size after catalysis (nm)
Au/Aerosil [a]	2.4	2.3 ± 0.5	10.1	
Au/Aerosil [b]	2.6	2.2 ± 0.5	10.5	
Au/silica gel	2.8	2.7 ± 1.1	8.5	8.5 ± 3.3
Au/SBA16	3.0	3.3 ± 0.6	4.6	3.3 ± 1.1
Au/MCF	2.8	3.0 ± 0.5	4.5	3.4 ± 1.1

[a] Au loading is 2.2 wt%.
[b] Au loading is 1.3 wt%.

aqueous solution under the pressure of O_2, but in the absence of the $NaHCO_3$ (particles grew to 4.4 nm). In the absence of HMF (all other reaction components were present), the particles remained small (3.0 nm). Surprisingly, in a solution with an initial pH of 8.5, particles were stable (3.5 nm instead of growth to 10.1 nm) if a diluted solution of NaOH was used as a base instead of $NaHCO_3$. It suggests that the nature of the anions present in the solution plays an important role in particle growth. In the absence of O_2 (under 10 bar N_2 and in the presence of all other reaction components), the particle growth was pronounced (to 14 nm), probably because without O_2 the pH remains high, while normally in the course of the reaction it decreases from pH 8.5 to 7. Hence, particle growth was enhanced by the presence of HMF and $NaHCO_3$, and also proceeded without catalytic action taking place.

The fact that large agglomerates of Au particles were formed during the reaction on Aerosil-supported samples suggests that some particles moved, collided and formed larger crystallites and aggregates thereof. Indeed, we observed that the reaction mixture of the Au/Aerosil catalyst after 2 h of catalysis and after filtration was pink (photo in the Supporting Information, S.2), hence Au nanoparticles had detached from the Aerosil support and were dispersed in the solution. However, the reaction mixture after 6 h of reaction was colorless, and elemental analysis of the post-reaction mixture showed no significant Au concentration in the reaction solution. No pink colour of the reaction solution was observed for Au/SBA16 and Au/MCF, while also for Au/silica gel coloration was observed. Hence Au colloids were only in solution during the first hours of reaction, and only for the Au/Aerosil and Au/silica gel samples that also showed the most pronounced Au particle growth. $NaHCO_3$ and/or HMF could act as capping agents, binding strongly to the nanoparticles, and weakening support-metal nanoparticle interaction. Though the reaction temperature is not very high, we suggest that movement of Au particles is the dominant particle growth mechanism, while the growth of the crystallites indicates that also Ostwald ripening or coalescence play a role.

3.3.2. The role of the support structure on Au particle stability

The particle growth was limited for both Au/MCF, with medium cage (26 nm) and neck (15 nm) sizes, and for Au/SBA16, with small cage (9 nm) and neck (7 nm) sizes. The growth was pronounced on

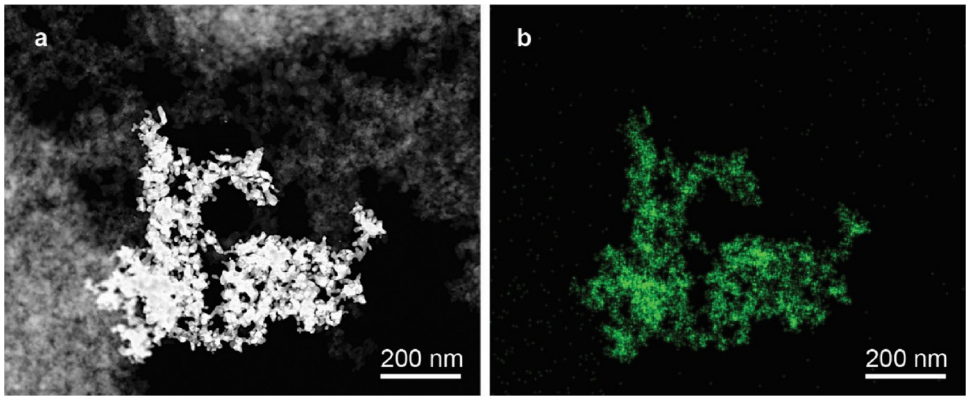

Fig. 6. a) High angle annular dark-field-scanning TEM image, and b) energy-dispersive X-ray spectroscopy image of the spent 2.2 wt% Au/Aerosil. In b) green represents the Au element (For interpretation of the references to colour in this figure legend, the reader is referred to the web version of this article).

silica gel, with 9 nm disordered pores, whereas the growth for Au/Aerosil with disordered pores of 50 nm was even more pronounced. The interparticle distance of Au nanoparticles on all different SiO_2 supports was in the range of 40–60 nm, hence the interparticle distances could not explain the differences in particle growth. With such large interparticle distances it is not likely that the movement of particles over the support surface plays an important role in the particle growth process [45], also as from the coloring of the solutions we can conclude that rather the movement of gold nanoparticles in the solution contributes to the redistribution of the gold. Our results also strongly suggest that pore *size* plays a role, as the open pore structure with 50 nm pores of the Aerosil leads to much larger particles than the sol-gel silica with disordered 9 nm pores. Also interesting is that the Au/silica gel shows much more pronounced particle growth than either Au/SBA16 or Au/MCF, while having a similar pore sizes as the first one and even much smaller pores than the latter. This clearly shows that also support pore *structure* is an important factor. We cannot fully exclude that other factors, such as pore corrugation and acidity, might play a role as well. Nevertheless, it is clear that diffusion of Au particles through the pore system, and hence Au particle growth, can be effectively counteracted by carefully selecting the silica support.

4. Conclusion

The activity and stability of SiO_2-supported Au nanocatalysts for the oxidation of HMF to FDCA were investigated for the first time. SiO_2-supported Au catalysts showed similar activities for this reaction as Au on carbon supports and reducible oxide supports reported in literature. Upon catalysis, Au nanoparticles supported on SiO_2 (Aerosil with 50 nm disordered pores) grew extensively. The particle growth under these reaction conditions is proposed to occur by diffusion of Au nanoparticles through the solution in the pores, and subsequent coalescence and growth into agglomerates containing 10–30 nm Au nanoparticles. A disordered silica with smaller pores led to less pronounced growth. However, growth was very limited for Au supported on ordered mesoporous SiO_2 supports (SBA16 and MCF). Hence, the choice of the support morphology is vital to the stability of supported Au nanoparticles during liquid phase oxidation reactions.

Acknowledgments

Wouter Lamme for the HAADF-STEM imaging, and NWO-Vici (16.130.344) for overall funding of the project are gratefully acknowledged. B.D. has received funding from the European Union's Horizon 2020 research and innovation programme under the Marie Skłodowska-Curie grant agreement No 703861.

Appendix A. Supplementary data

Supplementary material related to this article can be found, in the online version, at doi:https://doi.org/10.1016/j.apcata.2018.05.027.

References

[1] J.J. Bozell, G.R. Petersen, Green. Chem. 12 (2010) 539.
[2] R.A. Sheldon, Green. Chem. 16 (2014) 950–963.
[3] Z. Zhang, K. Deng, ACS Catal. 5 (2015) 6529–6544.
[4] Synvina, Joint Venture of BASF and Avantium, (2018) accessed via the webpage www. avantium. com in 2016.
[5] J.Cvd. Wall, E. Mazoyer, H.J. Baars, G.-J.M. Gruter, From Terephthalic Acid to 2,5-Furandicarboxylic Acid: An Industraial Perspective, in: S.S. Stahl, P.L. Alsters (Eds.), Liquid Phase Aerobic Oxidation Catalysis: Industrial Applications and Academic Perspectives, Wiley-VCH, Germany, 2016, p. 313.
[6] X. Han, L. Geng, Y. Guo, R. Jia, X. Liu, Y. Zhang, Y. Wang, Green. Chem. 18 (2016) 1597–1604.
[7] H. Ait Rass, N. Essayem, M. Besson, Green. Chem. 15 (2013) 2240.
[8] Y. Zhang, Z. Xue, J. Wang, X. Zhao, Y. Deng, W. Zhao, T. Mu, RSC Adv. 6 (2016) 51229–51237.
[9] C. Zhou, W. Deng, X. Wan, Q. Zhang, Y. Yang, Y. Wang, ChemCatChem 7 (2015) 2853–2863.
[10] H. Ait Rass, N. Essayem, M. Besson, ChemSusChem 8 (2015) 1206–1217.
[11] S. Siankevich, G. Savoglidis, Z. Fei, G. Laurenczy, D.T.L. Alexander, N. Yan, P.J. Dyson, J. Catal. 315 (2014) 67–74.
[12] B. Liu, Y. Ren, Z. Zhang, Green. Chem. 17 (2015) 1610–1617.
[13] B. Siyo, M. Schneider, J. Radnik, M.-M. Pohl, P. Langer, N. Steinfeldt, Appl. Catal. A. 478 (2014) 107–116.
[14] Z. Zhang, J. Zhen, B. Liu, K. Lv, K. Deng, Green. Chem. 17 (2015) 1308–1317.
[15] Y. Wang, K. Yu, D. Lei, W. Si, Y. Feng, L.-L. Lou, S. Liu, ACS Sustain. Chem. Eng. 4 (2016) 4752–4761.
[16] K. Gupta, R.K. Rai, A.D. Dwivedi, S.K. Singh, ChemCatChem 9 (2017) 2760–2767.
[17] D. Lei, K. Yu, M.-R. Li, Y. Wang, Q. Wang, T. Liu, P. Liu, L.-L. Lou, G. Wang, S. Liu, ACS Catal. 7 (2016) 421–432.
[18] J. Nie, J. Xie, H. Liu, J. Catal. 301 (2013) 83–91.
[19] G. Yi, S.P. Teong, Y. Zhang, Green. Chem. 18 (2016) 979–983.
[20] O. Casanova, S. Iborra, A. Corma, ChemSusChem 2 (2009) 1138–1144.
[21] J. Cai, H. Ma, J. Zhang, Q. Song, Z. Du, Y. Huang, J. Xu, Chem. Eur. J. 19 (2013) 14215–14223.
[22] N.K. Gupta, S. Nishimura, A. Takagaki, K. Ebitani, Green. Chem. 13 (2011) 824.
[23] S.E. Davis, B.N. Zope, R.J. Davis, Green. Chem. 14 (2012) 143–147.
[24] B. Siyo, M. Schneider, M.-M. Pohl, P. Langer, N. Steinfeldt, Catal. Lett. 144 (2014) 498–506.
[25] K.-Q. Sun, S.-W. Luo, N. Xu, B.-Q. Xu, Catal. Lett. 124 (2008) 238–242.
[26] S.E. Davis, L.R. Houk, E.C. Tamargo, A.K. Datye, R.J. Davis, Catal. Today 160 (2011) 55–60.
[27] Z. Miao, Y. Zhang, X. Pan, T. Wu, B. Zhang, J. Li, T. Yi, Z. Zhang, X. Yang, Catal. Sci. Technol. 5 (2015) 1314–1322.
[28] A. Villa, M. Schiavoni, S. Campisi, G.M. Veith, L. Prati, ChemSusChem 6 (2013) 609–612.
[29] S. Albonetti, A. Lolli, V. Morandi, A. Migliori, C. Lucarelli, F. Cavani, Appl. Catal., B. 163 (2015) 520–530.
[30] K. Gupta, R.K. Rai, S.K. Singh, ChemCatChem (2018).
[31] J. Gong, Chem. Rev. 112 (2012) 2987–3054.
[32] M. Valden, X. Lai, D.W. Goodman, Science (1998) 128.
[33] S. Biella, L. Prati, M. Rossi, J. Catal. 206 (2002) 242–247.
[34] K. Heidkamp, N. Decker, K. Martens, U. Prüße, K.-D. Vorlop, O. Franke, A. Stankowiak, Eur. J. Lipid Sci. Technol. 112 (2010) 51–57.
[35] M. Comotti, C. Della Pina, R. Matarrese, M. Rossi, Angew. Chem. Int. Ed. Engl. 43

(2004) 5812–5815.
[36] C. Xu, Z. Wang, X. Huangfu, H. Wang, RSC Adv. 4 (2014) 27337–27345.
[37] B. Donoeva, N. Masoud, P.E. de Jongh, ACS Catal. 7 (2017) 4581–4591.
[38] A. Mirescu, H. Berndt, A. Martin, U. Prüße, Appl. Catal., A. 317 (2007) 204–209.
[39] N. Thielecke, K.-D. Vorlop, U. Prüße, Catal. Today 122 (2007) 266–269.
[40] E. Gaigneaux, M. Devillers, S. Hermans, P.A. Jacobs, J. Martens, P. Ruiz, Belgium, July 11-15, 2010, Elsevier Science, Scientific Bases for the Preparation of Heterogeneous Catalysts: Proceedings of the 10th International Symposium, Louvain-La-Neuve (2010).
[41] R. van den Berg, G. Prieto, G. Korpershoek, L.I. van der Wal, A.J. van Bunningen, S. Laegsgaard-Jorgensen, P.E. de Jongh, K.P. de Jong, Nat. Commun. 7 (2016) 13057.
[42] T.M. Eggenhuisen, G. Prieto, H. Talsma, K.P. de Jong, P.E. de Jongh, J. Phys. Chem. C 116 (2012) 23383–23393.
[43] P. Schmidt-Winkel, W.W. Lukens, D. Zhao, P. Yang, B.F. Chmelka, G.D. Stucky, J. Am. Chem. Soc. 121 (1999) 254–255.
[44] G. Prieto, M. Shakeri, K.P. de Jong, P.E. de Jongh, ACS Nano 8 (2014) 2522–2531.
[45] G. Prieto, J. Zecevic, H. Friedrich, K.P. de Jong, P.E. de Jongh, Nat. Mater. 12 (2013) 34–39.
[46] P. Munnik, M.E. Velthoen, P.E. de Jongh, K.P. de Jong, C.J. Gommes, Angew. Chem. Int. Ed. Engl. 53 (2014) 9493–9497.
[47] R. Mueller, H.K. Kammler, K. Wegner, S.E. Pratsinis, Langmuir 19 (2003) 160–165.
[48] X.Y. Liu, A.Q. Wang, X.F. Yang, T. Zhang, C.Y. Mou, D.S. Su, J. Li, Chem. Mater. 21 (2009) 410–418.
[49] A. Jentys, PCCP 1 (1999) 4059–4063.
[50] Y.Y. Gorbanev, S.K. Klitgaard, J.M. Woodley, C.H. Christensen, A. Riisager, ChemSusChem 2 (2009) 672–675.
[51] J.R. Regalbuto, K.P.d. Jong (Ed.), Synthesis of Solid Catalysts, Wiley-VCH Verlag GmbH & Co, Weinheim, 2009.